Supporting Information

Large-scale Synthesis of $LiNi_{0.75}Fe_{0.25}PO_4$ Covalently Anchored on Graphene Nanosheets for Remarkable Electrochemical Water Oxidation†

Shaojun Ma,[ab] Qing Zhu,[ab] Li Chen,[b] Wenlou Wang*[abcd] and Dongming Chen[a]

[a] Department of Chemical Physics, University of Science and Technology of China, Hefei, Anhui 230026, P. R. China

[b] Nano Science and Technology Institute, University of Science and Technology of China, Collaborative Innovation Center of Suzhou Nano Science and Technology, Suzhou, Jiangsu, 215123, P. R. China

[c]Collaborative Innovation Center of Suzhou Nano Science and Technology, Suzhou, Jiangsu, 215123, P. R. China

[d]National Synchrotron Radiation Laboratory, University of Science and Technology of China, Hefei, Anhui 230029, P. R. China

*Correspondence to: wlwang@ustc.edu.cn

Materials and Preparation of the catalysts

The $LiNi_{1-x}Fe_xPO_4$/GO hybrid were synthesized by a facile solvothermal method using $LiOH•H_2O$, $FeSO_4•7H_2O$, $NiSO_4•6H_2O$, H_3PO4 and graphene oxide (GO) as raw materials. Firstly, 0.03mol $LiOH•H_2O$ was dissolved 20 mL GO solution (4 mg/mL) solution. Simultaneously, 0.0025 mol $FeSO_4•7H_2O$, 0.0075 mol $NiSO_4•6H_2O$ and 0.01 mol H_3PO_4 were dissolved into a mixed solvent of glycol/H_2O (V_1:V_2 = 8:3) under continuous stirring for 1h. Subsequently, $LiOH•H_2O$/GO solutions was added to the above mixture dropwise with vigorous stirring. After stirring, the suspension obtained was rapidly transferred into a Teflon lined stainless steel reaction vessel and sealed tightly, which was subsequently heated at 180 ^oC for 10 h. After reaction, as-obtained precipitate was filtered, washed with deionized water and ethanol several times, and dried at 80 ^oC in vacuum for 6 h. Finally, the as-prepared powders were annealed at 400 ^oC for 1 h, 500 ^oC for 2h in an N_2 atmosphere. The commercial RuO_2 and IrO_2 used in this work were purchased from Sigma-Aldrich without any further purification.

Characterizations

Powder X-ray diffraction patterns were collected using a Rigaku/Max-3A X-ray diffractometer with Cu Kα radiation (λ = 1.54178 Å). The SEM images were taken using a field-emission scanning electron microscope (JSM-6701F, JEOL) operated at an accelerating voltage of 5 kV. Energy-dispersive X-ray spectroscopy (EDS) analysis was performed on a JEOL-2010 microscope with an accelerating voltage of

200 kV. All the samples were prepared by depositing a drop of diluted suspensions in ethanol on a carbon-film-coated copper grid. Raman spectra were measured with a Perkin-Elmer 400F Raman Spectrometer using a 514.5 nm laser beam. Nitrogen adsorption measurements were performed at 77 K using a Micromeritics ASAP 2020 system utilizing Brunauer–Emmett–Teller (BET) calculations for surface area. The X-Ray absorption near-edge structure (XANES) spectra have been recorded on beamline U19 at the National Synchrotron Radiation Laboratory, China. The beam from a bending magnet was monochromatized with a varied line-spacing plane grating monochromator and refocused by a toroidal mirror. XANES spectra were recorded the surface sensitive total electron yield (TEY) from the sample as function of the incoming photon energy. The data were collected in a mode of sample drain current under a vacuum lower than 5×10^{-7} Pa.

Electrode preparation

Electrochemical experiments were analyzed using a traditional three-electrode configuration cell, which was connected to a CHI660E electrochemical analyzer (Shanghai Chenhua Limited, China). A platinum wire was used as the auxiliary electrode and a double-junction Ag/AgCl (KCl saturated) electrode was used as the reference electrode with 1 M KOH as electrolyte. Both the counter and reference electrodes were rinsed with distilled water and dried with compressed nitrogen prior to the measurements. The glassy carbon electrodes (PINE, 5 mm diameter, 0.196 cm^2) loaded with catalysts were used as the working electrodes. The working

electrodes were prepared as follows: the catalysts (4mg) were suspended in 2 ml of ethanol and 20 μL Nafion (5%), the resulting solution was referred to as the "catalyst ink" and was sonicated until excellent dispersion was achieved. Then a 30 μL aliquot of the ink was dropped onto the glassy carbon rotating disk electrode, yielding an approximate loading of 300 μg cm^{-2}. After the ink was dried, the electrode was visually inspected to ensure uniform film formation. Carbon cloth (CC) were cleaned carefully with acetone, and then washed in succession with ethanol and deionized water for three times. The catalyst-loaded carbon cloth anode was prepared by mixing the prepared sample (90 wt.%) and conductive adhesive (10 wt.%) slurry coated onto 1 cm × 4 cm carbon cloths wrapped with hydrophobic adhesive tape except for a part of 1 × 1 cm^2 as the working electrode. The loading of catalyst was achieved by typical drop-casting method with a mass loading ~0.6 mg cm^{-2} and dried under ambient conditions. The catalyst's activity towards OER was tested in O_2-saturated electrolyte solution by linear sweep voltammetry (LSV) from 0 to 0.7 V versus Ag/AgCl, which was performed at 5 mV s^{-1} after purging the electrolyte with O_2 gas for 30 min at room temperature. The working electrode was rotated at 1600 rpm during testing. The accelerated stability tests were performed in 1 M KOH at room temperature by potential cycling between 0 and 0.6 V versus Ag/AgCl at a sweep rate of 100 mV/s for 2000 cycles. At the end of the cycles, the resulting electrodes were used for LSV at a sweep rate of 5mV/s. For samples loaded on CC, chronoamperometric measurements were done at η = 300 mV. ECSA was determined by measuring the

capacitive current associated with double-layer charging from the scan-rate dependence of CVs. The potential window of CVs was -0.2 to -0.1 V versus Ag/AgCl (1 M KOH). The double-layer capacitance (C_{dl}) was estimated by plotting the ΔJ ($j_a - j_c$) at -0.15 V versus Ag/AgCl (1 M KOH) against the scan rate.

RHE calibration

In all measurements, we used Ag/AgCl (KCl saturated) as the reference electrode. It was noted that the current density was normalized to the geometrical area and the measured potentials vs Ag/AgCl were calibrated with respect to a reversible hydrogen electrode (RHE) scale according to the Nernst equation ($E_{RHE} = E_{Ag/AgCl} + 0.059 \times pH + 0.197$); the overpotential ($\eta$) was calculated according to the following formula: η (V) = $E_{RHE} - 1.23$ V.

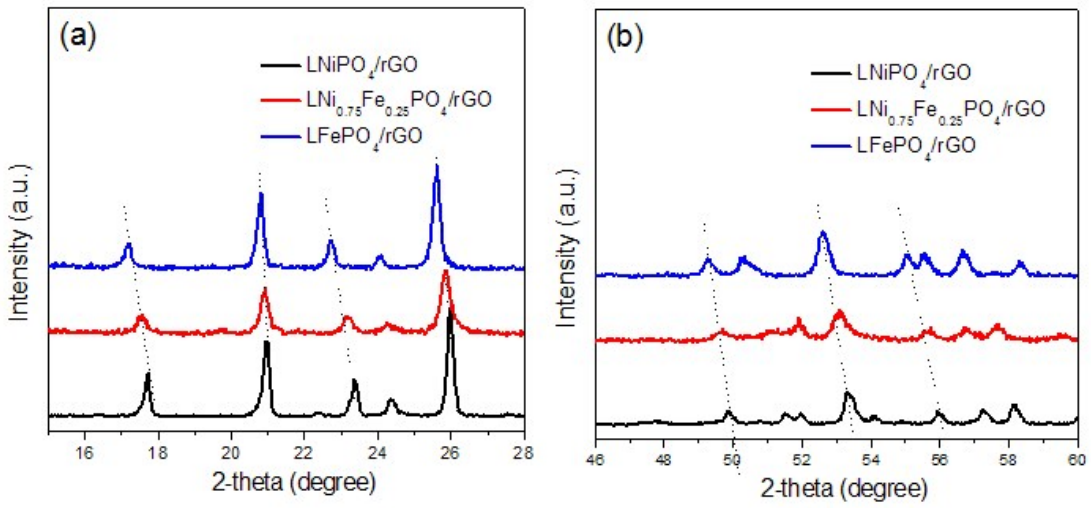

Fig. S1 XRD patterns of $LiNi_xFe_yPO_4$/rGO with different compositions.

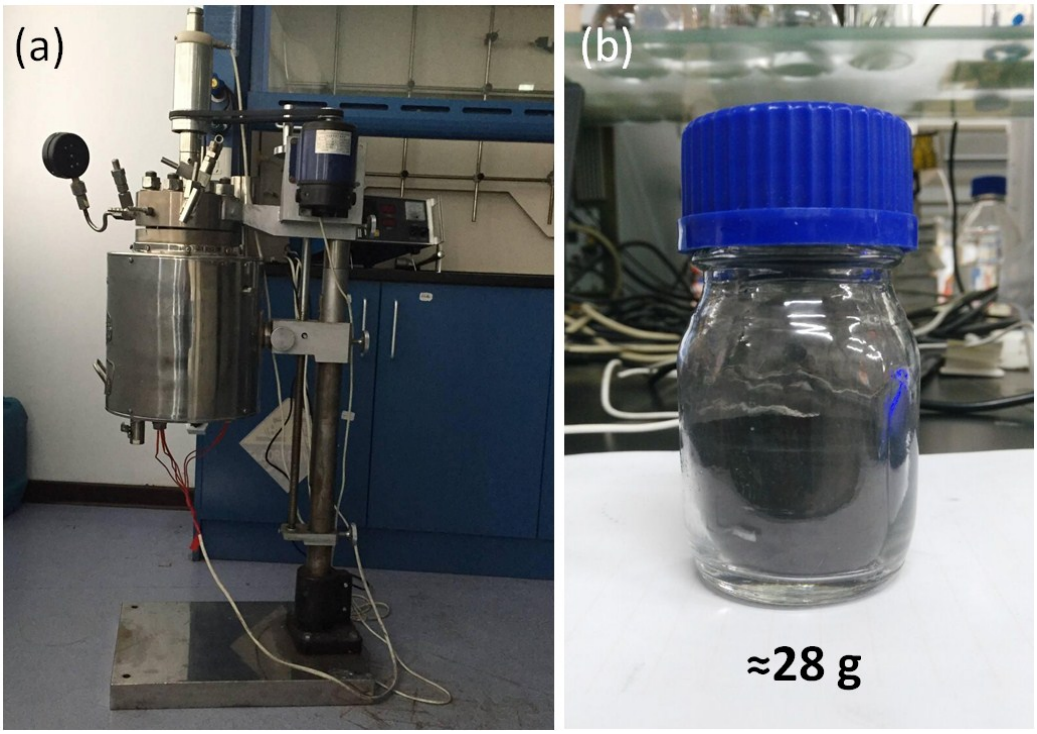

Fig. S2 (a) Photograph of Teflon-lined stainless steel autoclaves with 2000 mL volumes. The photograph was taken with permission of the Wang's Lab at the University of Science and Technology of China (USTC). (b) Photographs of $LiNi_{0.75}Fe_{0.25}PO_4$/rGO sample obtained at tens of grams level by one-pot synthesis using a 2000 mL Teflon-lined stainless steel autoclave.

It is worth mentioning that our $LiNi_{0.75}Fe_{0.25}PO_4$/rGO can be fabricated on a large scale by using a large autoclave (2000 mL) for the hydrothermal treatment, and highly OER active $LiNi_{0.75}Fe_{0.25}PO_4$/rGO composite can be obtained on the tens of grams level (see photograph in Fig. S2b).

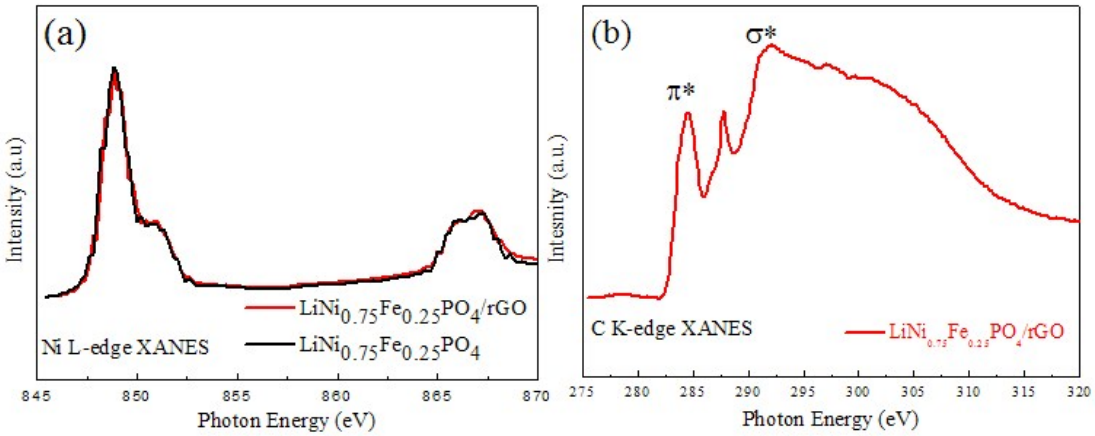

Fig. S3 XANES spectra of $LiNi_{0.75}Fe_{0.25}PO_4$/rGO and carbon-free $LiNi_{0.75}Fe_{0.25}PO_4$ at the (a) Ni L-edge and (b) C K-edge recorded in TEY mode.

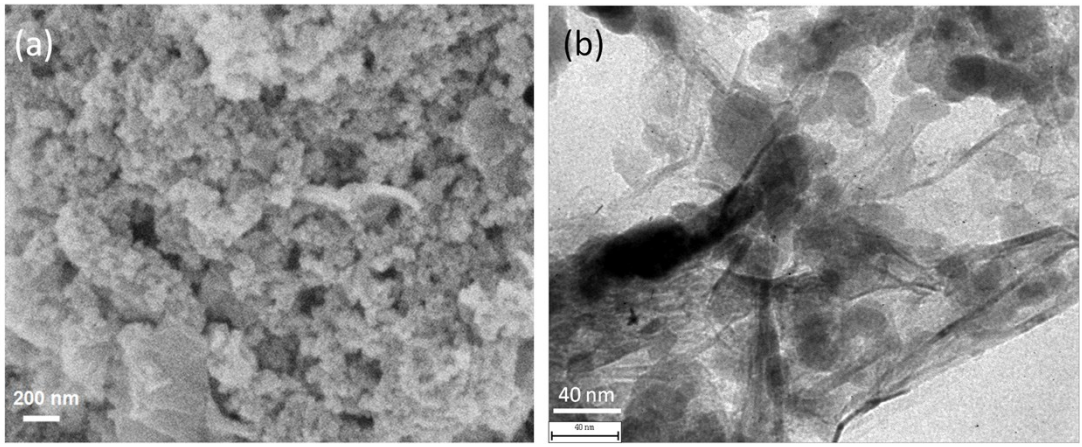

Fig. S4 (a) SEM and (b) TEM image of $LiNi_{0.75}Fe_{0.25}PO_4$/rGO after 2000th stability tests.

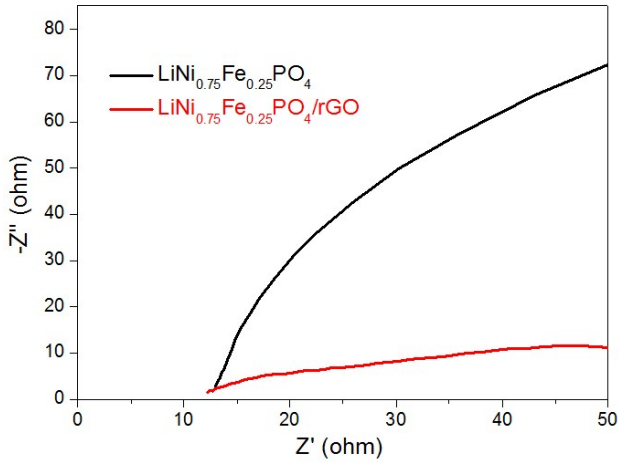

Fig. S5 Electrochemical impedance spectroscopy of $LiNi_{0.75}Fe_{0.25}PO_4$/rGO composites and $LiNi_{0.75}Fe_{0.25}PO_4$ at 1.53 V vs. RHE.

In general, ohmic series resistance (R_s) includes the solution resistance, electrode electrolyte interface resistance and electrode material collector contact resistance, which is not primarily determined by the activity catalyst. The charge transfer resistance (R_{ct}) related to the electrocatalytic kinetics, which is determined by internal resistance of catalyst and could be calculated from the diameter of the semicircles in the low frequency zone of electrochemical impedance spectroscopy (EIS) measurements. The $LiNi_{0.75}Fe_{0.25}PO_4$ anchoring on graphene sheets dramatically reduce charge transfer resistance (R_{ct}), the R_{ct} resistance decreased from positive infinity to 65 ohm after hybriding with graphene, clearly demonstrating an increase in the electrical conductivity of the $LiNi_{0.75}Fe_{0.25}PO_4$/rGO composite as compared to pristine $LiNi_{0.75}Fe_{0.25}PO_4$ and enhanced electron transfer kinetics during the OER process.

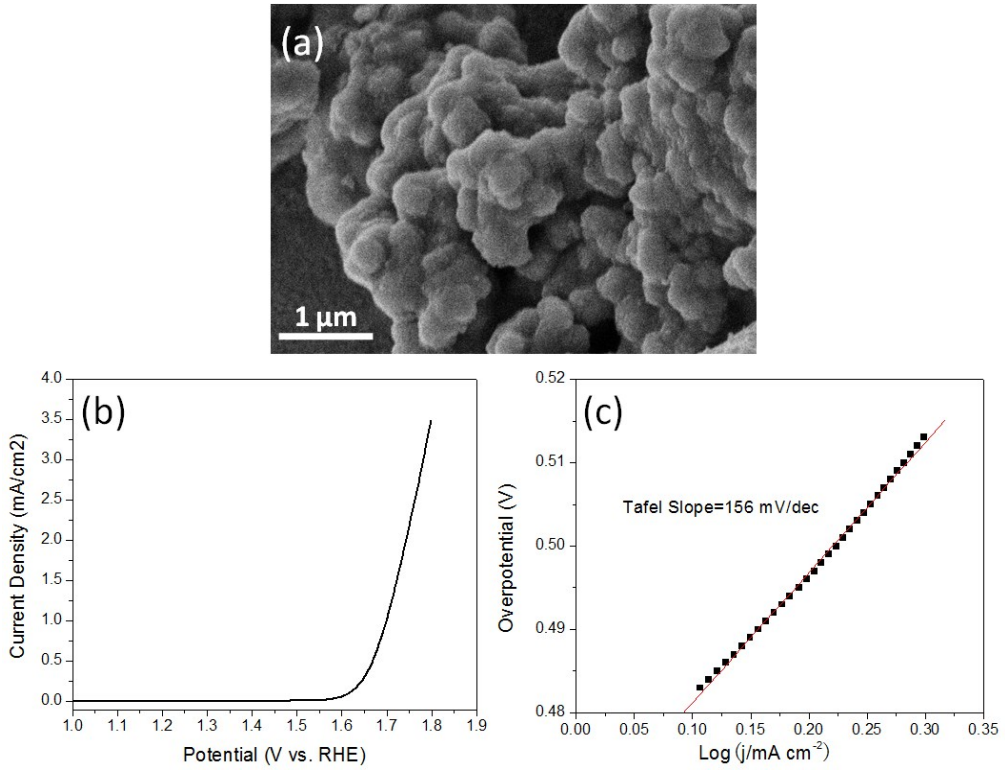

Fig. S6 (a) SEM image of $LiNi_{0.75}Fe_{0.25}PO_4$ without rGO coating (b) Linear-sweep voltammogram showing the electrocatalysis of water oxidation by $LiNi_{0.75}Fe_{0.25}PO_4$ and (c) corresponding Tafel plots obtained in O_2-saturated KOH (1 M) at a scan rate of 5 mV s^{-1}.

Table S1.Comparison of OER performance in alkaline media of with other non-noble metal electrocatalysts ([a]Catalysts directly grown on current collector).

Catalyst	Tafel Slope (mV/dec)	η(@10 mA/cm^2)	Electrolyte	Ref.
$LiFe_xNi_{1-x}PO_4$/rGO/GC	47	0.295	1 M KOH	This work
$Zn_xCo_{3-x}O_4$NWs/Ti[a]	51	0.320	1 M KOH	*Chem. Mater*., 2014, **26**, 1889.[S1]
PNG-$NiCo_2O_4$/GC	156	0.349	0.1 M KOH	*ACS Nano*, 2013, **7**,10190.[S2]
Co_3O_4/$NiCo_2O_4$/GC	88	0.340	1 M KOH	*J. Am. Chem. Soc*., 2015, **137**, 5590.[S3]
Co_3O_4-NA/Cu foil[a]	70	0.290	0.1 M KOH	*J. Am. Chem. Soc*., 2014, **136**, 13925.[S4]
NiFe-LDH/CNT/GC	35	0.308	0.1 M KOH	*J. Am. Chem. Soc*., **2013**, **135**, 8452.[S5]
P-g-C_3N_4/CF[a]	61.6	0.4	0.1 M KOH	*Angew. Chem. Int. Ed*., 2015, **54**, 4646.[6]
Ni@NC/GC	44	0.390	0.1 M KOH	*Adv. Energy Mater*., 2014, **5**, 1401660.[S7]
CoMn LDH/GC	43	0.325	1 M KOH	*J. Am. Chem. Soc*., 2014, **136**, 1648.[S8]
Mn_3O_4/$CoSe_2$/GC	49	0.450	0.1 M KOH	*J. Am. Chem. Soc*., 2012, **134**, 2930.[S9]
CoCo-NS/GC	40	0.32	1 M KOH	*Nat. Commun*., 2014, **5**, 4477.[S10]
$CoSe_2$/N-Graphene/GC	~40	0.366	0.1 M KOH	*ACS Nano*, 2014, **8**, 3970.[S11]
N/C/GC	N.A.	0.380	0.1 M KOH	*Nat. Commun*., 2013, **4**, 2390.[S12]

Ni–Fe alloy/GC	42	0.375	0.1 M KOH	*Chem. Commun*., 2015, **51**, 1922.[S13]
NiCo LDHs /GC	40	0.367	1 M KOH	*Nano Lett*., 2015, **15**, 1421.[S14]
Ni-Co hollow sponges/GC	64	0.362	0.1 M KOH	*Chem. Commun*., 2015, **51**, 7851.[S15]
$Ba_{0.5}Sr_{0.5}Co_{0.8}Fe_{0.2}O_{3-\delta}$/GC	60	~0.36	0.1 M KOH	*Nat. Commun*., 2013, **4**, 2439.[S16]
Au@Co_3O_4/GC	60	~0.38	0.1 M KOH	*Adv. Mater*., 2014, **26**, 3950.[S17]
α-$Ni(OH)_2$ hollow spheres/GC	42	0.331	0.1 M KOH	*J. Am. Chem. Soc*., 2014, **136**, 7077.[S18]
Ultrathin $NiCo_2O_4$nanosheets/GC	30	0.320	1 M KOH	*Angew. Chem. Int. Ed.*, 2015, **54**, 7399.[S19]
FeNC sheets/NiO/GC	76	0.39	0.1 M KOH	*Angew. Chem. Int. Ed*., 2015, **54**, 1.[S20]
Fe-mCo_3O_4/GC	60	0.380	1 M KOH	*Chem. Commun*., 2014, **50**, 10122.[S21]
Annealed C-Co NPs/GC	N.A.	0.39	0.1 M KOH	*J. Am. Chem. Soc*. 2015, **137**, 7071.[S22]
Mn-Co oxide/NCNTs/GC	N.A.	~0.44	0.1 M KOH	*J. Am. Chem. Soc*., 2014, **136**, 7551.[S23]
Fe-Co_3O_4/GC	N.A.	0.486	0.1 M KOH	*Chem. Mater*., 2014, **26**, 3162.[S24]
Co-P film[a]	47	0.345	1 M KOH	*Angew. Chem. Int. Ed*., 2015, **54**, 6251.[S25]
Co_xO_y/NC/GC	74.8	0.43	0.1 M KOH	*Angew. Chem. Int. Ed*., 2014, **53**, 8508.[S26]
Amorphous Ni-Co Oxide/Au-films[a]	39	0.325	1 M NaOH	*ACS Nano*, 2014, **8**, 9581.[S27]
CoO/NG/GC	71	0.34	1 M KOH	*Energy Environ. Sci*., 2014, **7**, 609.[S28]
Ni-Co LDH/CP[a]	40	0.367	1 M KOH	*Nano Lett*., 2015, **15**, 1421.[S29]

$LiCo_{0.33}Ni_{0.33}Fe_{0.33}O_2$/GC	46	0.295	1M KOH	*Nat. Commum*., 2015, **5**, 4345.[S30]
CoP NR/C/GC	71	0.32	1 M KOH	*ACS Catal*., 2015, **5**, 6874.[31]
CoS_2/N,S-GO/GC	75	0.38	0.1 M KOH	*ACS Catal*., 2015, **5**, 3625.[S32]
$Ni_{30}Fe_7Co_{20}Ce_{43}O_x$/GC	70	0.41	1 M NaOH	*Energy Environ. Sci*., 2014, **7**, 682.[S33]
Ni–Co Hydroxide/GC	65	0.46	0.1 M KOH	*Adv. Funct. Mater*., 2014, **24**,4698.[S34]
nNiFe LDH/NGF/GC	45	0.337	0.1M KOH	*Adv. Mater*., 2015, **27**, 4516–4522.[S35]

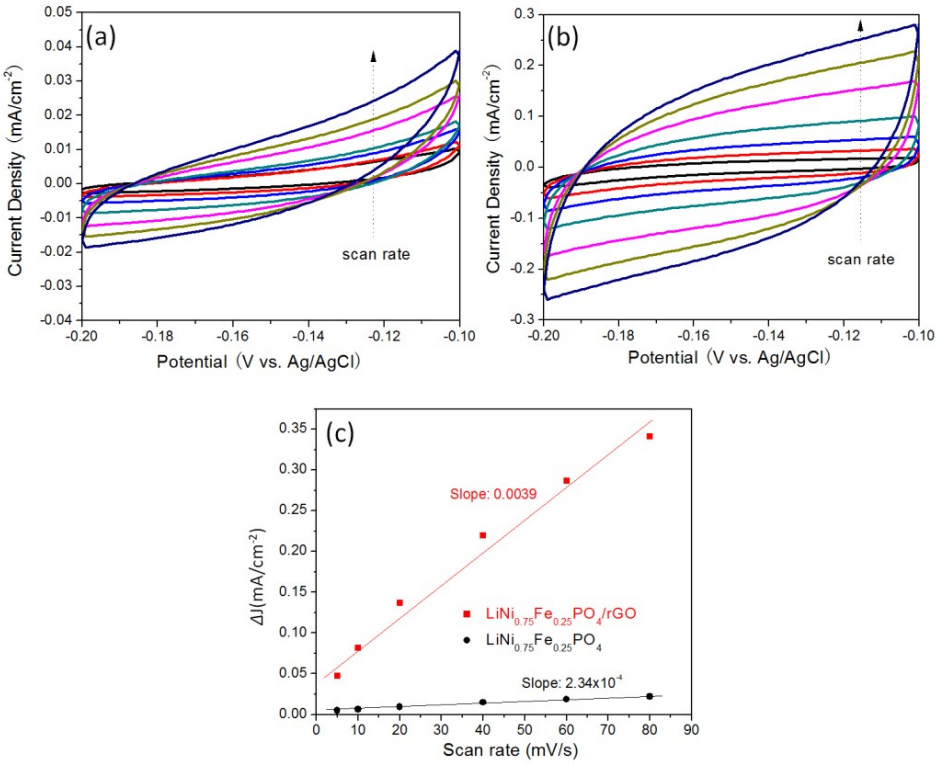

Fig. S7 Cyclic voltammograms of $LiNi_{0.75}Fe_{0.25}PO_4$ (a) and $LiNi_{0.75}Fe_{0.25}PO_4$/rGO (b) composite measured at different scanning rates (5, 10, 20, 40, 60, 80 mV/s) in 1 M KOH. (c) Corresponding charging current density differences (ΔJ = ja − jc) plotted against scan rates.

To figure out different catalytic performance of porous catalysts, electrochemical double-layer capacitances (C_{dl}) were measured to evaluate the relative differences in electrochemically active surface areas and roughness factors of various catalysts via a simple cyclic voltammetry (CV) method. The relative value of electrochemically active surface area can be obtained by normalization of C_{dl}. The halves of the positive and negative current density differences ($\Delta j = j_a - j_c$) at a given potential (0.15 V vs. Ag/AgCl) are plotted against the CV scan rates, which can be well fitted using a linear function where the slopes are the so-called C_{dl}.

References:

S1 X. Liu, Z. Chang, L. Luo, T. Xu, X. Lei, J. Liu, X. Sun, *Chem. Mater.*, 2014, **26**, 1889.

S2 S. Chen, S. Qiao, *ACS Nano*, 2013, **7**, 10190.

S3 H. Hu, B. Guan, B. Xia, X. Lou, *J. Am. Chem. Soc.*, **2015**, 137, 5590.

S4 T. Y. Ma, S. Dai, M. Jaroniec, S. Z. Qiao, *J. Am. Chem. Soc.*, 2014, **136**, 13925.

S5 M. Gong, Y. Li, H. Wang, Y. Liang, J. Wu, J. Zhou, J. Wang, T. Regier, F. Wei, H. Dai, *J. Am. Chem. Soc*., 2013**, 135**, 8452.

S6 T. Y. Ma, J. R. Ran, S. Dai, M. Jaroniec andS. Z. Qiao, *Angew. Chem. Int. Ed*., 2015, **54**, 4646.

S7 J. W. Ren, M. Antonietti, T. P. Fellinger, *Adv. Energy Mater.*, 2014, **5**, 1401660.

S8 F. Song and X. Hu, *J. Am. Chem. Soc*., 2014, **136,** 16481.

S9 M. R. Gao, Y. F. Xu, J. Jiang, Y. R. Zheng and S. H. Yu, J. *Am. Chem. Soc.*, 2012, **134**, 2930.

S10 F. Song and X. Hu, *Nat. Commun*., 2014, **5**, 4477.

S11 M. R. Gao, X. Cao, Q. Gao, Y. F. Xu, Y. R. Zheng, J. Jiang and S. H. Yu, *ACS Nano*, 2014, **8**, 3970.

S12 Y. Zhao, R. Nakamura, K. Kamiya, S. Nakanishi and K. Hashimoto, *Nat. Commun*. 2013, **4**, 2390.

S13 T. N. Kumar, S. Sivabalan, N. Chandrasekaran and K. L. Phani, *Chem. Commun*., 2015, **51**, 1922.

S14 H. Liang, F. Meng, M. Caban-Acevedo, L. Li, A. Forticaux, L. Xiu, Z. Wang and

S. Jin, *Nano Lett.*, 2015, **15**, 1421.

S15 C. Z. Zhu, D. Wen, S. Leubner, M. Oschatz, W. Liu, M. Holzschuh, F. Simon, S. Kaskelb and A. Eychmuller, *Chem. Commun*., 2015, **51**, 7851.

S16 A. Grimaud, K. J. May, C. E. Carlton, Y. L. Lee, M. Risch, W. T. Hong, J. G. Zhou and S. H. Yang, *Nat. Commun*. 2013, **4**, 2439.

S17 Z. B. Zhuang, W. C. Sheng and Y. S. Yan, *Adv. Mater*., 2014, **26**, 3950–3955.

S18 M. R. Gao, W. C. Sheng, Z. B. Zhuang, Q. R. Fang, S. Gu, S. Jiang and Y. S. Yan, *J. Am. Chem. Soc*., 2014, **136**, 7077.

S19 J. Bao, X. D. Zhang, B. Fan, J. J. Zhang, M. Zhou, W. L. Yang, X. Hu, H. Wang, B. C. Pan and Y. Xie, *Angew. Chem. Int. Ed.*, 2015, **54**, 7399.

S20 J. Wang, K. Li, H. X. Zhong, D. Xu, Z. L. Wang, Z. Jiang, Z. J. Wu and X. B. Zhang. *Angew. Chem. Int. Ed*., 2015, **54**, 1.

S21 C. L. Xiao, X. Y. Lu and C. Zhao, *Chem. Commun*., 2014, **50**, 10122.

S22 L. H. Wu, Q. Li, C. H. Wu, H. Y. Zhu, A. Mendoza-Garcia, B. Shen, J. H. Guo, and S. H. Sun, *J. Am. Chem. Soc*., 2015, **137**, 7071.

S23 A. Q. Zhao, J. Masa, W. Xia, A. Maljusch, M. G. Willinger, G. Clavel, K. P. Xie, R. Schlögl, W. Schuhmann and M. Muhler, *J. Am. Chem. Soc.*, 2014, **136**, 7551.

S24 T. Grewe, X. H. Deng and H. Tüysüz, *Chem. Mater.*, 2014, **26**, 3162.

S25 N. Jiang, B. You, M. L. Sheng, Y. J. Sun, *Angew. Chem. Int. Ed.*, 2015, 54, 6251.

S26 J. Masa, W. Xia, I. Sinev, A. Q. Zhao, Z. Y. Sun, S. Grtzke, P. Weide, M. Muhler and W. Schuhmann, *Angew. Chem. Int. Ed.*, 2014, **53**, 8508.

S27 Y. Yang, H. L. Fei, G. D. Ruan, C. S. Xiang and J. M. Tour, *ACS Nano*, 2014, **8**,

9581.

S28 S. Mao, Z. H. Wen, T, Z. Huang, Y. Houa, J. H. Chen, *Energy Environ. Sci*., 2014, **7**, 609.

S29 H. F. Liang, F. Meng, M. Caban-Acevedo, L. S. Li, A. Forticaux, L. C. Xiu, Z. C. Wang and S. Jin, *Nano Lett.*, 2015, **15**, 1421.

S30 Z. Y. Lu, H. T. Wang, D. S. Kong, K. Yan, P. C. Hsu, G. Y. Zheng, H. B. Yao, Z. Liang, X. M .Sun and Y. Cui, *Nat. Commum*., 2015, **5**, 4345.

S31 J. F. Chang, Y. Xiao, M. L. Xiao, J. J. Ge, C. P. Liu and W. Xing, *ACS Catal*., 2015, **5**, 6874.

S32 P. Ganesan, M. Prabu, J. Sanetuntikul and S. Shanmugam, *ACS Catal*., 2015, **5**, 3625.

S33 J. A. Haber, Y. Cai, S. Jung, C. G. Xiang, S. Mitrovic, T. Jin, A. T. Bellbd and J. M. Gregoire, *Energy Environ. Sci*., 2014, **7**, 682.

S34 Z. L. Zhao, H. X. Wu, H. L. He, X. L. Xu and Y. D. Jin, *Adv. Funct. Mater*., 2014, **24**, 4698.

S35 C. Tang, H. S. Wang, H. F. Wang, Q. Zhang, G. L. Tian, J. Q. Nie and F. Wei., *Adv. Mater*., 2015, **27**, 4516.